Improving the efficiency of photovoltaic cells embedded in floating buoys

Vahdat Nazerian[1], Hossein Asadollahi[1], Tole Sutikno[2,3]

[1]Department of Electrical Engineering, Faculty of Engineering and Technology, University of Mazandaran, Babolsar, Iran
[2]Master Program of Electrical Engineering, Faculty of Industrial Technology, Universitas Ahmad Dahlan, Yogyakarta, Indonesia
[3]Embedded System and Power Electronics Research Group, Yogyakarta, Indonesia

Article Info	ABSTRACT
	Solar cells are used to power floating buoys, which is one of their applications. Floating buoys are devices that are placed on the sea and ocean surfaces to provide various information to the floats. Because these cells are subjected to varying environmental conditions, modeling and simulating photovoltaic cells enables us to install cells with higher efficiency and performance in them. The parameters of the single diode model are examined in this article so that the I-V, P-V diagrams, and characteristics of the cadmium telluride (CdTe) photovoltaic cell designed with three layers (CdTe, CdS, and SnOx) can be extracted using a solar cell capacitance simulator (SCAPS) software, and we obtain the parameters of the single diode model using the ant colony optimization (ACO) algorithm. In this paper, the objective function is root mean square error (RMSE), and the best value obtained after 30 runs is 5.2217×10^{-5} in 2.46 seconds per iteration, indicating a good agreement between the simulated model and the real model and outperforms many other algorithms that have been developed thus far. The above optimization with 200 iterations, a population of 30, and 84 points was completed on a server with 32 gigabytes of random-access memory (RAM) and 30 processing cores.

Corresponding Author:

Vahdat Nazerian
Department of Engineering and Technology, Electrical Engineering, University of Mazandaran
Babolsar, Iran
Email: v.nazerian@umz.ac.ir

1. INTRODUCTION

Floating buoys are navigational aids that specify information such as waterways, borders, signs, and ocean states [1]. These vessels collect the necessary information from the seas and their surroundings using sensors embedded in them, and send it to the control center via a communication antenna after processing the data [2]–[4]. This data can be used for ocean monitoring, climate change research, and marine science [3]. The buoys' equipment requires a power source to function, and because they are located far from the coast and on the water surface, renewable energy is the best option for them.

Solar energy is a type of renewable energy that is free and available everywhere [5]. Floating buoys use one to several solar cells to supply their required electricity, depending on their type and application [1], [6]. When these photovoltaic (PV) cells are placed on the surface of the oceans and waters, the temperature of the modules drops due to surface evaporation as well as wind and sea storms, and their radiation angle may also change, resulting in a decrease in cell performance and efficiency [4]. These cells are manufactured using various technologies such as monocrystal, polycrystal, and thin film [7]–[9], so it is necessary to use efficient methods to simulate and model them so that we can select an optimal cell with high performance and weather resistance. The single-diode model is one of the simulation models, and many researchers extracted its

parameters using various algorithms [10]–[16]. The more accurate the algorithm's results, the more accurate the orbital model parameters will be. As a result, we investigate the efficiency and optimization of the ant colony algorithm (ACO) to extract the characteristics of the single diode model in this article.

Dorigo proposed the ant colony optimization algorithm, as a doctoral thesis. The behavior of ants to find the shortest path between the nest and the food source inspired this algorithm. When moving around, many types of ants secrete a substance called pheromone, which is understandable and appealing to other ants. The amount of pheromone in the shortest path between the nest and the food increases over time, and as a result, the number of ants drawn to this shorter path increases. This cycle is repeated until the majority of ants take the shorter route. Because none of the ants were able to find the shortest path on their own and this was the result of agent cooperation, this algorithm can be classified as a swarm intelligence algorithm [17]–[20]. Figure 1 depicts the equipment and various parts of one type of floating buoy [21].
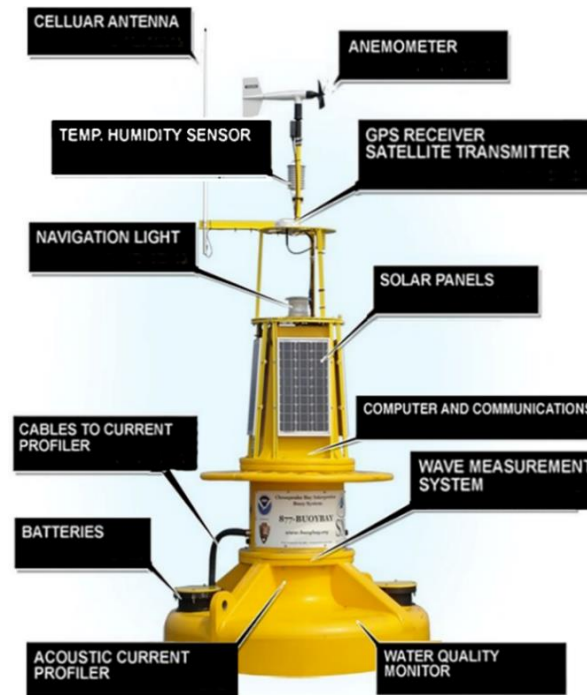

Figure 1. Different parts of a smart buoy

2.   MODELLING A SOLAR CELL AND THE GOVERNING EQUATIONS

The purpose of this work is to match the characteristic curve (P-V, I-V) of the simulation model with the characteristic curve of the real cell under different environmental conditions [22]. The most common method is using an electrical equivalent circuit based on the diode model and simulates the cell's p-n junction [14], [15]. Many researchers have presented many models, the simplest of which is the single diode model, which we will examine in the following circuit model. When not exposed to radiation, the solar cell behaves like a diode, with the current-voltage equation as in (1):

$$I_D = I_S \left[e^{\frac{V_D}{\eta V_T}} - 1 \right] \xrightarrow{V_T = \frac{kT}{q}} I_D = I_S \left[e^{\frac{qV_D}{\eta kT}} - 1 \right] \tag{1}$$

where k=1.38064×10⁻²³ J/k is Boltzmann's constant, q=1.602176634×10⁻¹⁹ (in Coulombs) is the electric charge of an electron, η is the diode's ideal coefficient, V_T (mV) is the thermal voltage, V_D (V) is the diode voltage, I_S (A) is the reverse saturation current, I_D is the diode current [23], [24]. Figure 2 depicts the current-voltage density diagram of a solar cell in the absence of radiation. When exposed to radiation, however, a current appears in the cell as a result of the photovoltaic phenomenon, which is referred to as the radiation current and is represented by the symbol I_{Ph}. In circuit models, this current is considered a dependent current source, and its current size is directly proportional to the light irradiated to the cell, changing as a linear coefficient with the light [14], [25].
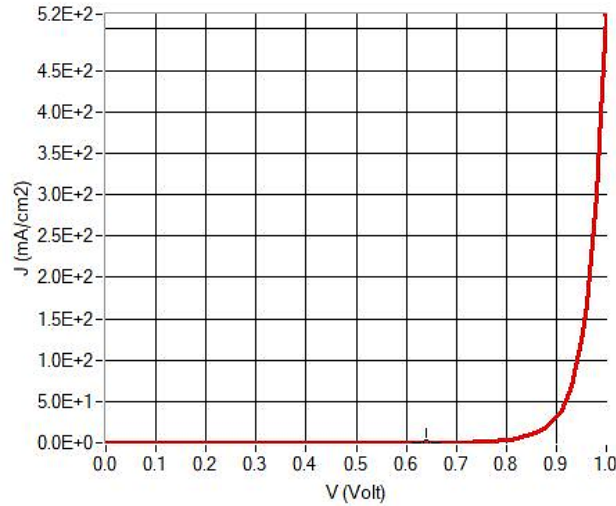
Figure 2. I-V curve without irradiation

2.1. Single-diode model

A cell can be modeled using a light-dependent current source in parallel with a diode, as shown in Figure 3. It has the current-voltage equation as in (2) and (3) [10], [13], [14], [23], [25]–[29].

$$I = I_{Ph} - I_{D_1} - I_P \tag{2}$$

$$I = I_{Ph} - I_{S_1}\left[e^{\frac{q(V+R_SI)}{\eta_1 kT}} - 1\right] - \frac{V+R_SI}{R_P} \tag{3}$$

In this model, there are two parasitic resistances, R_s and R_p, where:
− The series resistance is the result of the semiconductor resistance, the resistance between the contacts and the cell, and the internal resistance of the metal contacts. The series resistance is a challenge at high current densities.
− The parallel resistance is the result of leakage currents, particularly at the cell edges [10], [14], [30]. Also, in (2), I_P (A) is the parallel resistance's current, I_{Ph} (A) is the PV current and I is the output current of the model. In the single-diode model, 5 parameters, including $\eta_1, I_{S_1}, I_{Ph}, R_P, R_S$ are required to complete the I-V characteristic.
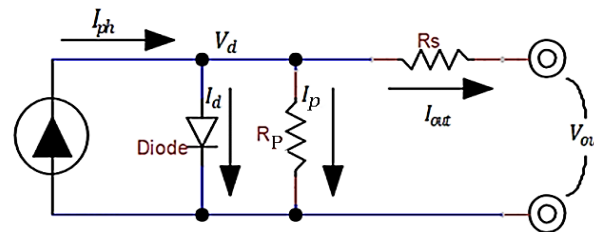

Figure 3. Equivalent circuit of the single-diode model

2.2. Cost function of root mean square error

Root mean square error (RMSE), as an essential tool, serves to evaluate the performance quality of predictive models and is widely used for model assessment and comparison. It is simplicity and interpretability make it a valuable metric for reporting in research papers, enabling readers to assess the accuracy and reliability of the discussed models. RMSE measures the error between two sets of data and typically compares the predicted values with the observed or measured values. In this article, this parameter serves as our objective function, and its relationships are described as (4).

$$RMSE = \sqrt{\frac{1}{N}\sum_{i=0}^{N-1}(I_i - I_{(Vi)})^2} \qquad\qquad (4)$$

In which N is the number of measure currents, I_i is the experimental current, and I_{V_i} is the current obtained using the algorithm and RMSE is the root mean square error [14], [23], [29], [31], [32].

2.3. Fill factor

The short-circuit current (I_{SC}) and open-circuit voltage (V_{OC}) represents the maximum current and voltage that a cell can generate, respectively. However, at these two points, the output power is zero. The fill factor, denoted as FF, quantifies the conversion efficiency of a solar cell in terms of how effectively it can convert solar radiation into usable energy. This parameter is defined as the ratio of the maximum power output of the solar cell to the product of I_{SC} and V_{OC} [10]:

$$FF = \frac{P_{MP}}{V_{OC} \times I_{SC}} = \frac{V_{MP} \times I_{MP}}{V_{OC} \times I_{SC}} \qquad\qquad (5)$$

Also, I_{MP} (A) and V_{MP} (V) represent the voltage and current of the maximum point.

3.   ANT COLONY OPTIMIZATION ALGORITHM

The ACO, also known as ant colony optimization, is based on the natural behavior of ant colonies and the worker ants who live in them. In an ant colony, the process of locating food sources is highly optimized. When ants begin to search for food, they will naturally find a "logical" and "optimal" path from their nest to food sources. In other words, the ant population is always able to find the best path to provide the necessary food resources. Ant colony optimization is based on simulating such optimal behavior [33]. It should be noted that the exact name of this algorithm is ant colony optimization, which most people refer to as ant algorithm or ant colony algorithm. Consider two ants traveling from their nest to a food source in opposite directions. Ants secrete a trace of pheromone into the environment as they move towards a food source, which naturally decays over time. The ant that takes the shortest path to the food source begins the return journey to the nest before the other ants. In such a case, on the way back to the nest, this ant begins releasing pheromone into the environment again, thereby strengthening the pheromone trail left in the shortest path. Other ants follow the strongest pheromone trail in the environment instinctively and reinforce the pheromone trail in this path. After a certain period of time, not only does the pheromone trail in the shortest path disintegrate, but it is also strengthened by the accumulation of pheromone trails from other ants. The path with the strongest pheromone trace becomes the default path for ants to travel from the colony to the food source [34], [35].

Figure 4 depicts how to find the shortest path. Pseudo-code of the ACO is given in the following:
a) Parameters of the ACO are adjusted and the pheromone traces are initialized.
b) Until the termination condition is not met:
   Firstly, it generates candidate solutions and then, using local search, determines which pheromones need to be updated. This step is optional and not present in some implementations using ant colony algorithms. Finally, the pheromones are updated.
c) If the termination condition is met, stop the algorithm; otherwise, repeat the above steps.

Figure 5 shows the ACO flowchart [36], [37]. In the following, we will provide a brief explanation of each of these stages. Initially, in the candidate solution generation stage, a set of m artificial ants generate candidate solutions for the optimization problem using elements from a finite set of available candidate solution components $C = \{c_{ij}\}, i = 1, \ldots, n, j = 1, \ldots, |D_i|$. This stage begins with the generation of a partial candidate solution $s^p = \emptyset$. Subsequently, in the following steps, the generated s^p is expanded by adding a component from the set of feasible neighbors $N(s^p) \subseteq C$.
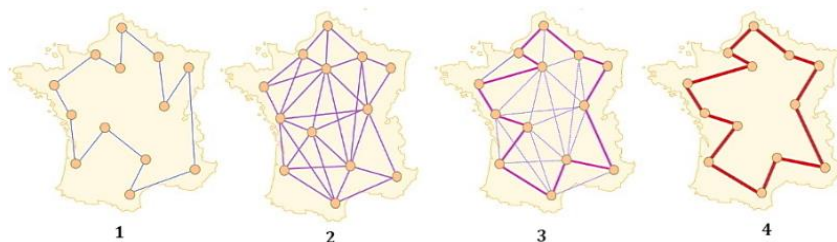

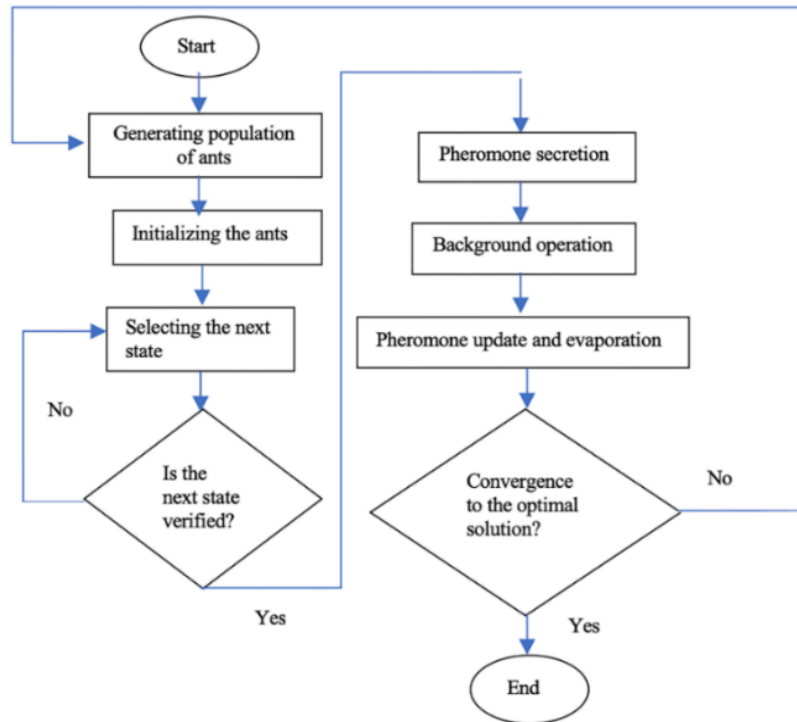Figure 4. Pheromone evaporation after multiple iterations of ACO

Figure 5. ACO flowchart

The process of generating candidate solutions can be viewed as a path in the structural graph $G_C(V, E)$. In other words, expanding the optimal solution refers to determining possible movement paths for the artificial ant in the pheromone model's structural graph. Through this approach, the neighborhoods of the partial candidate solution are explored to identify the best path toward the global optimal solution. The permissible paths in the graph G_C are implicitly defined by the candidate solution generation mechanism. The candidate solution generation mechanism defines the set of feasible neighbors $N(s^p) \subseteq C$ for each partial solution separately. The rules for selecting a component from the set of feasible neighbors, in different implementations of ant colony algorithms, may vary. However, the most well-known rule is associated with the ant system algorithm [20], [33].

$$P(c_{ij}|s^p) = \frac{\tau_{ij}^\alpha \times \eta(c_{ij})^\beta}{\sum_{c_{il} \in N(s^p)} \tau_{il}^\alpha \times \eta(c_{il})^\beta} \forall c_{ij} \in N(s^p) \tag{6}$$

In this regard, τ_{ij} represents the pheromone values associated with the component c_{ij}, and $\eta(.)$ is a function that assigns a so-called heuristic value to each candidate solution $c_{ij} \in N(s^p)$ at each stage of candidate solution generation. The heuristic values generated by the function $\eta(.)$ are referred to as Heuristic Information. Additionally, the parameters α and β are positive-valued parameters that determine the relative importance (weight) of the pheromone information (values of candidate solution variables) and the heuristic information in determining the probability value of the above-mentioned relationship [17]–[20].

In the local search stage, depending on the implemented ant colony algorithm, additional processes may be necessary to ensure optimal algorithm performance after candidate solutions are generated but before pheromones are updated. Therefore, this stage is optional. The nature of these processes is intensive, meaning they cannot be performed by just one artificial ant. These processes are referred to as auxiliary operations or daemon actions. The most common background operation in ant colony algorithm-based algorithms is the deployment of local search on the generated candidate solutions. For example, locally optimized solutions can be used to make decisions about updating pheromone values [18], [19].

In the final stage, the objective of updating pheromones is to increase the pheromone values associated with good and optimal candidate solutions while decreasing the pheromone values associated with bad solutions. This is achieved through two major processes: i) decreasing the pheromone values associated with all candidate solutions through the process of pheromone evaporation and ii) increasing the pheromone values associated with candidate solutions belonging to the set of good solutions, denoted as S_{upd}. These two processes are controlled by the following relationship, referred to as the pheromone updating rule.

$$(1 - \rho) \times \tau_{ij} + \rho \sum_{s \in S_{upd}|c_{ij} \in s} F(s) \rightarrow \tau_{ij} \tag{7}$$

The first part of this relationship controls the process of pheromone evaporation, which decreases the pheromone values of all candidate solutions. The second part increases the pheromone values only for the candidate solutions belonging to the set of good solutions, S_{upd}. In this context, S_{upd} includes the candidate solutions that have high fitness, meaning they are closer to the global optimal solution. The parameter $\rho \in (0,1)$, known as the evaporation rate, and $F: S \rightarrow R_0^+$, known as the fitness function, are involved. In simpler terms, this process leads to an increase in the pheromone values associated with the ants that are on the best available paths towards the optimal solution (i.e., closer to the optimal solution) and have higher fitness (lower cost or higher benefit). As a result, other ants also converge towards these paths.

The presence of the pheromone evaporation parameter is essential in ant colony algorithm implementations to prevent rapid and premature convergence. The evaporation parameter provides a type of forgetting mechanism in the optimization process, emphasizing more on exploring and searching new areas in the search space of the implemented ant colony algorithms [19], [20], [33], [36], [37]. The advantages of the ant colony algorithm method can be summarized as follows [18], [20], [34]:

a) Cooperative group collaboration among ants for generating optimal solutions demonstrates the inherent nature of parallelism and solidarity in this method.
b) Positive feedback created through pheromone dissemination in the environment leads to rapid convergence to good solutions for the optimization problem.
c) It is suitable for dynamic applications that require quick adaptation to environmental changes.
d) Convergence to the optimal solution is guaranteed.

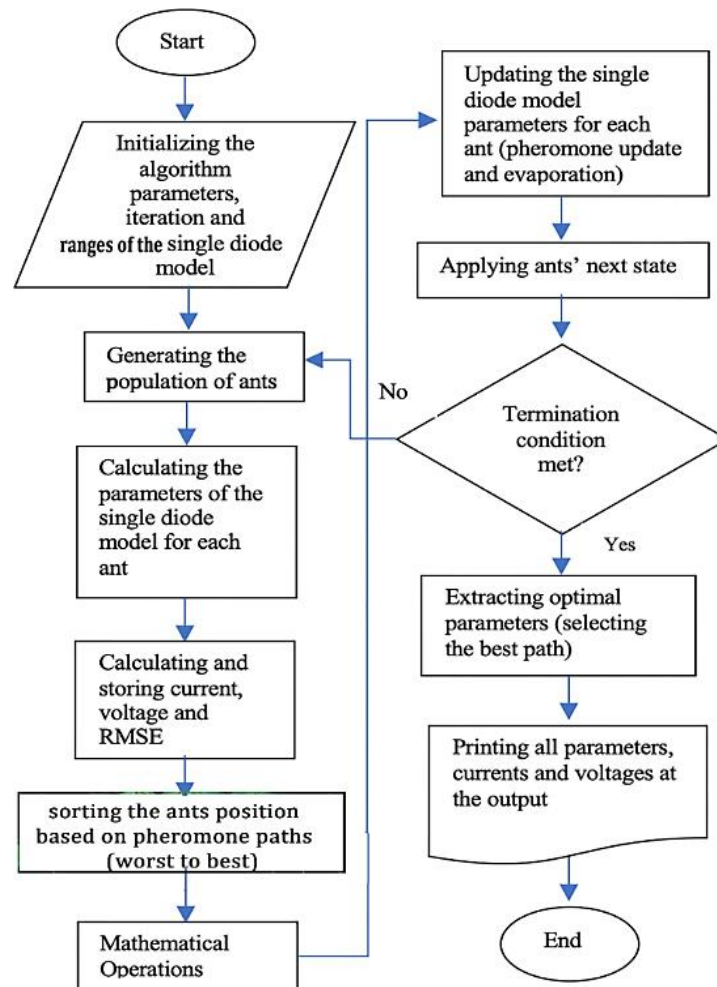This algorithm is rewritten as in Figure 6 to extract the components of the single-diode model.

Figure 6. ACO flowchart for extracting the single-diode model components

4. RESULTS AND DISCUSSION

In this section of the article, we first explain how to use the ACO algorithm to obtain the characteristics of a single diode equivalent circuit, and then describe the test conditions, data, and results obtained according to the categories listed below. To find the parameters of the equivalent circuit, we first extract the graphs and data of the desired cell under specific laboratory conditions (such as radiation, temperature, and so on), then we go to the optimization algorithm and define a range for the diode model components.

4.1. Experimental conditions and characteristics

The desired algorithm obtains the currents using the defined formulas and puts them in the objective function. The objective function applies a specific mathematical operation between the laboratory data and the algorithmic data and a number is extracted. This process continues until the number obtained from the objective function is the smallest available value, this value will be our final solution and the parameters that produced this number are the characteristics of our single diode model. The categories mentioned above are:

a) The employed solar cell is a *Cadmium Telluride* (CdTe) with an area of 1 cm^2.
b) The currents and powers are obtained in 1 cm^2 of the cell of interest (*current density*=A/cm^2).
c) Irradiation is constant equal to 1000 W/m^2 and temperature is 33 °C (306.15 K).
d) The processing server has 30 processing cores and 32 GB RAM Intel Xeon E5-2650 v4 2.20 GHz x64, RAM EDO 32 GB.
e) The employed algorithm for simulation is ACO with a population of 30 ants, 200 iterations, and 30 runs.
f) 84 points are measured with 0.01 steps.
g) I_{SC} and V_{OC} of the cell are 0.02413144 (A) and 0.857103 (V).
h) The experimental data is extracted using SCAPS, where its selected cell is CdTe comprising three layers of SnOx, CdS, and CdTe [38]. Table 1 represents the characteristics of the PV cell.

Table 1. Characteristics of the cell of interest in SCAPS

Layer name	Layer1	Layer2	Layer3
Name	CdTe	CdS	SnOx
Thickness (μm)	4.000	0.025	0.500
The layer is pure A: $y = 0$, uniform	0.000	0.000	0.000
Semiconductor property P of the pure material	Pure A ($y = 0$)	Pure A ($y = 0$)	Pure A ($y = 0$)
Bandgap (eV)	1.500	2.400	3.600
Electron affinity (eV)	3.900	4.000	4.000
Dielectric permittivity (relative)	9.400	10.000	9.000
CB effective density of states (1/ cm^3)	$8 \times 10^{+17}$	$2.200 \times 10^{+18}$	$2.200 \times 10^{+18}$
VB effective density of states (1/ cm^3)	$1.8 \times 10^{+19}$	$1.8 \times 10^{+19}$	$1.8 \times 10^{+19}$
Electron thermal velocity (cm/s)	$1 \times 10^{+7}$	$1 \times 10^{+7}$	$1 \times 10^{+7}$
Hole thermal velocity (cm/s)	$1 \times 10^{+7}$	$1 \times 10^{+7}$	$1 \times 10^{+7}$
Electron mobility (cm²/Vs)	$3.2 \times 10^{+2}$	$1 \times 10^{+2}$	$1 \times 10^{+2}$
Hole mobility (cm²/Vs)	$4 \times 10^{+1}$	$2.5 \times 10^{+1}$	$2.5 \times 10^{+1}$
Shallow uniform donor density ND (1/cm^3)	0.000	$1.1 \times 10^{+18}$	$1 \times 10^{+17}$
Shallow uniform acceptor density NA (1/cm^3)	$2.4 \times 10^{+14}$	0.000	0.000

Layer contact	Left contact (back)	Right contact (front)
Thermionic emission/surface recombination velocity (cm/s):		
Electrons	$1 \times 10^{+7}$	$1 \times 10^{+7}$
Holes	$1 \times 10^{+7}$	$1 \times 10^{+7}$
Metal work function (eV)	5.000	4.100
Majority carrier barrier height (eV):		
Relative to EF	0.400	0.100
Relative to EV or EC	0.1045	0.0199
Optical filter:	Transmission	Reflection
Filter mode	(80% mirror)	(10% mirror)
Illuminated from	Right (n-Side) or front	

***Other parameters that are not in the table were considered zero.

4.2. Results and diagrams

Table 2 specifies the estimation range of the parameters for optimization where the minimum value of most elements is 10^{-12}, which is considered to be zero. Most of these ranges are defined based on international publications [12], [23], [27], [29]. Also, the maximum PV current is 1.5 times the short circuit current of the tested cell. Following an extensive optimization process involving 200 iterations, utilizing 30 ants and conducting 30 runs, a clear conclusion was drawn. It was determined that the desired results were achieved precisely during the 199th iteration, utilizing the 8th ant, and in the first run. The corresponding RMSE values associated with these outcomes have been documented in Table 3 for reference and analysis.

Table 4 showcases the current, voltage, and maximum power values acquired at the point of interest, and these figures are compared to the corresponding values from the experimental case. The findings reveal a remarkable level of accuracy, as the obtained results exhibit minimal deviation from the actual measurements. This outcome reinforces the reliability and precision of the conducted analysis, affirming the validity of the acquired data. In the following, we examine other experimental and algorithmic curves.

Table 2. Results and range of 7 unknown parameters using ACO

Range	R_S (Ω)	η_1	I_{Ph} (A)	I_{S1} (μA)	R_P (Ω)
Min value	0	1	0	0	0
Max value	1	2.5	0.03619716615	2	1000
results	2.9765×10^{-4}	2.0307	0.024265	2.4489×10^{-3}	994.6844

$** I_{Ph} = (1.5) \times (I_{SC}) \rightarrow I_{SC} = 0.02413144410 \rightarrow I_{Ph} = 0.03619716615$
$**10^{-12} \cong 0 \rightarrow$ lower boundaries

Table 3. RMSE, population and desired iteration

Parameter	Iteration number	Population number	RMSE
Value	199	8	5.2217×10^{-5}

Table 4. Maximum experimental and algorithmic current, voltage, and power

Parameter	V_{MPP}	I_{MPP}(A)	P_{MPP}(w)
Algorithmic values	0.72	0.0218611	0.01574
Experimental values	0.715420	0.0219611711	0.015711461028

4.2.1. I-V and P-V curves

The high compatibility between the curves is prominently demonstrated in Figures 7 and 8, which showcase their exceptional alignment. This compatibility is attributed to the remarkably low RMSE value, indicating the minimal deviation between the curves. Additionally, the superior accuracy achieved through optimization using the ACO algorithm further enhances the robustness and reliability of the curves' alignment.
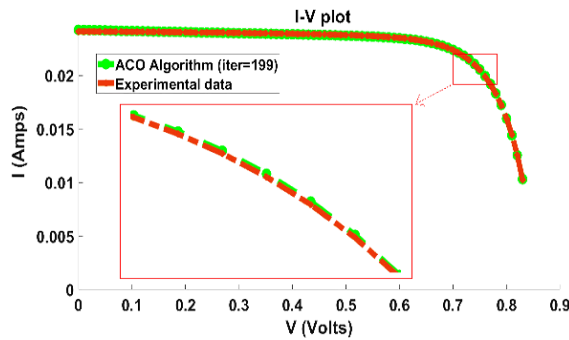

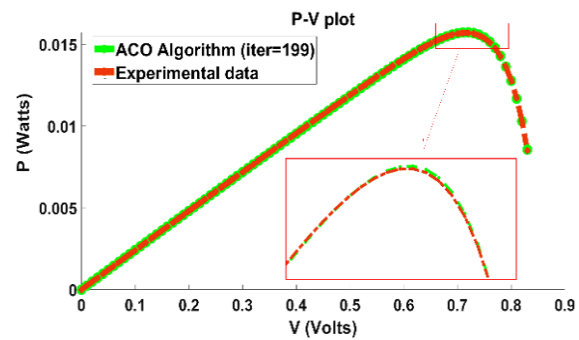Figure 7. Agreement of experimental and algorithmic I-V

Figure 8. Agreement of experimental and algorithmic P-V

4.2.2. RMSE-iteration curve

Figure 9 depicts the value of RMSE in each iteration round. As shown in the figure, as the iteration round increases, the quantity of RMSE should decrease, and from the 190th iteration onwards, it reaches a stability and stability in the solution with only slight variations. Increasing the iteration time beyond 200 has a negligible influence on the optimization results, roughly 1×10^{-5}.

4.2.3. Time iteration curve

Figure 10 depicts the algorithm's run time during each iteration round. According to the graph, each iteration round takes roughly 2-3 seconds on average. The algorithm appears to be performing more difficult computations as the algorithm time has grown between the 80 to 110 iteration rounds. This rise in time can also be seen in the internal figure, and the chart is broken in the region of 80 to 110. The times of each round

of repetition are combined together in this figure, and the total duration of completing the algorithm in 200 rounds of iterations is roughly 492.36 seconds.
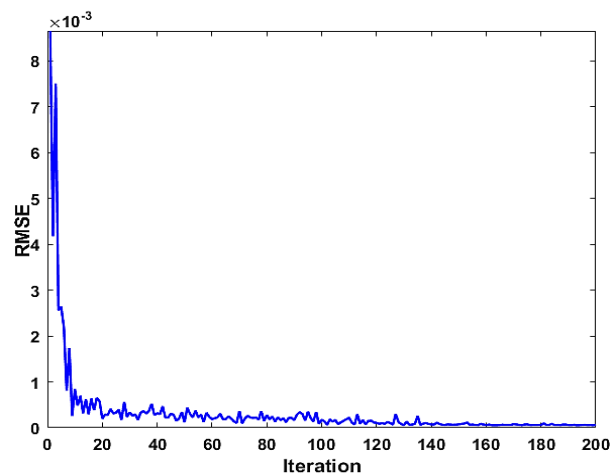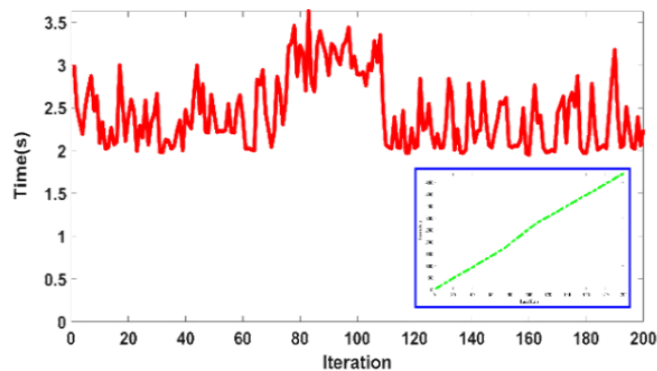

Figure 9. RMSE-iteration curve

Figure 10. Time-iteration curve

4.3. Effect of algorithm components on the optimization results
4.3.1. Increasing iteration round
One of the parameters impacting the algorithm's findings is the iteration round. Figures 9 and 11 show that increasing the iterations increases the accuracy and agreement of the results and output graphs with the experimental values and graphs until the desired method has reached stability and stability in the results. However, once stability is achieved, extending the iteration round has no effect on the RMSE value.

4.3.2. Increasing population
Another component affecting our outcomes is the size of the population included in the optimization. Each ant, according to the ACO algorithm, produces a chemical known as a pheromone in the path it chooses and passes. Any path with a higher concentration of pheromone is a shorter path, and more ants pass through it. As a result, the more ants that engage in the optimization, the results would be more accurate, and the ensuing graphs are the most compatible with the cell's experimental conditions. Figure 12 depicts this. Another point that was investigated and should be considered is that, similar to the iteration round, an increase in population affects the optimization results up to a certain amount, and anything more than that amount not only has little effect, but also has an effect on the duration of the optimization of the result.

The outcomes of the experiment involving 11 ants are presented in Table 5, revealing notably positive results. The data showcased in the table demonstrates the effectiveness of utilizing this particular number of ants in achieving favorable outcomes. These findings contribute valuable insights into the potential of optimizing the experiment by employing an adequate number of ants for enhanced performance and reliable results.
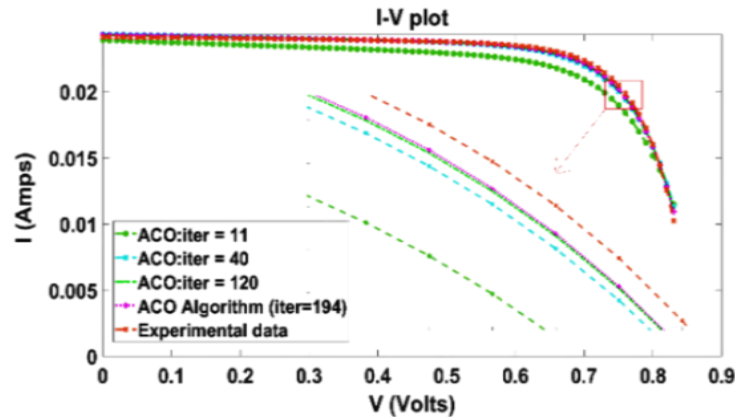
Figure 11. Comparing I-V curves of different iteration rounds with each other and experimental curve of the cell
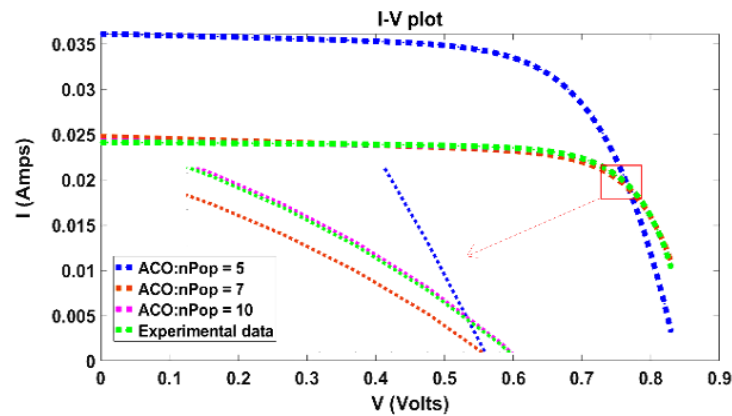

Figure 12. Comparing I-V curves of different populations with each other and the experimental curve of the cell

Table 5. Results and ranges of 7 unknown parameters with 11 ants

Parameter	value	Parameter	value
I_{Ph} (A)	0.02428	Population number	6
I_{S1} (µA)	4.6044×10^{-3}	Total population	11
R_P (Ω)	999.9998	Iteration	200
R_S (Ω)	2.2499×10^{-7}	RMSE	7.019×10^{-5}
η_1	2.1189	Time	193.213
Iteration number	200		

4.4. Comparing the results with other algorithms

The superiority of the ACO method over other algorithms in the single-diode model is clearly demonstrated by the results presented in Table 6. With its exceptional performance, the ACO method emerges as an ideal choice for modeling and simulations, offering a combination of efficiency and accuracy. Researchers can confidently utilize this algorithm to achieve reliable and precise outcomes in their studies and applications.

4.5. Sparsity of RMSE and time in 30 runs

Based on the findings depicted in Figure 13 and Table 7, a substantial proportion of the RMSE values obtained from 30 runs fall within the range of 1.6×10^{-4} to 2.2×10^{-4}, indicating a high level of consistency and accuracy. Additionally, it is noteworthy that approximately four runs yielded RMSE values as low as 10^{-5}, further highlighting the exceptional performance of the algorithm. These impressive RMSE ranges clearly surpass the performance of alternative algorithms, demonstrating the superiority of the method in achieving precise and reliable results.

Table 6. Comparing RMSE of the algorithms with each other

| Algorithm Name	Iteration/population	RMSE	Algorithm name	Iteration/population	RMSE
ACO	200/30	5.2217×10^{-5}	Performance-guided JAYA (PGJAYA) [39]	50000/20	9.8602×10^{-4}
Artificial bee colony (ABC) [40]	10000/150	9.862×10^{-4}	Chaotic whale optimization algorithm (CWOA) [41]	10000/150	9.98678×10^{-4}
Ensemble particle swarm optimizer (EPSO) [29]	200/30	8.0621×10^{-4}	GOFPANM [42]	10000/10	9.8602×10^{-4}
Fractional chaotic ensemble particle swarm optimizer (FC-EPSO1) [29]	200/30	7.7301×10^{-4}	Self-adaptive teaching-learning-based optimization (SATLBO) [43]	50000/40	9.8602×10^{-4}
FC-EPSO2 [29]	200/30	7.7339×10^{-4}	Enhanced leader particle swarm optimization (ELPSO) [44]	100/991	7.7301×10^{-4}
FC-EPSO3 [29]	200/30	7.7309×10^{-4}	Hybrid firefly and pattern search (HFAPS) [45]	5000/50	9.8602×10^{-4}
Multiple learning backtracking search algorithm (MLBSA) [46]	50000/50	9.8602×10^{-4}	Artificial bee swarm optimization (ABSO) [47]	5000/30	9.9124×10^{-4}
Time varying acceleration coefficients PSO (TVACPSO) [48]	100/1000	7.7301×10^{-4}	Hybrid particle swarm optimization and simulated annealing (HPSOSA) [31]	100/500	7.7301×10^{-4}
Coyote optimization algorithm (COA) [13]	1000/5 packs with 20 coyotes in each group	7.7547×10^{-4}	Grey wolf optimizer and cuckoo search (GWOCS) [49]	500/30	9.8607×10^{-4}
Tree growth algorithm (TGA) [27]	500/500	9.75053×10^{-4}	Logistic chaotic Rao-1 optimization algorithm (LCROA) [23]	1000/10	7.490069×10^{-4}
Enhanced Harris hawks optimization (EHHO) [50]	2000/30	9.8602×10^{-4}	Enhanced Lévy flight bat algorithm (ELBA) [51]	50000/20	9.860219×10^{-4}
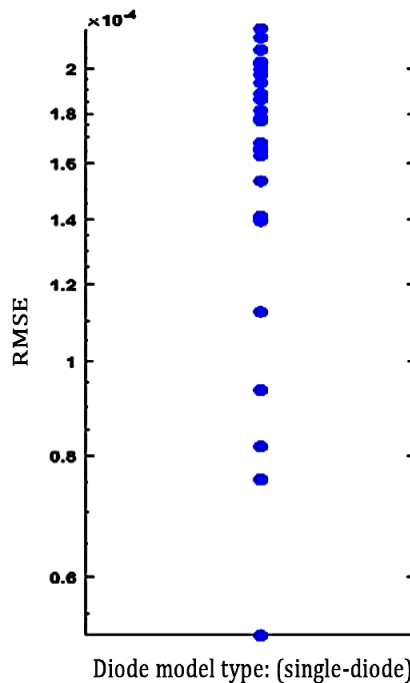
Figure 13. RMSE sparsity in single-diode model

Table 7. RMSE of the single-diode ACO

Type of equivalent circuit	Min RMSE	Max RMSE	Avg RMSE
Single diode	5.2217 e-05	2.199 e-04	1.6068 e-04

Figure 14 shows the time distribution of the algorithm execution in the single-diode model in 30 runs. Also, based on this figure, it can be seen that the running time of the algorithm varies from 440 to 480 seconds on average. The information presented in this figure provides researchers and practitioners with valuable insights into the amount of time required to run the algorithm.
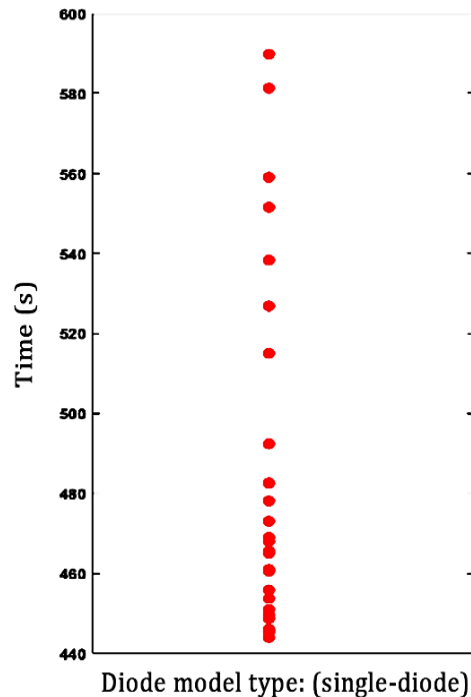

Figure 14. Time sparsity in the single-diode model

5. CONCLUSION

Floating buoys serve a significant role in ocean and sea navigation by transmitting vital information to vessels and their control centers. These buoys require a power supply to measure and transmit data so that the sensors, processing unit, communications antennae, warning lights, and other components can function. Because these buoys will stay on the water's surface for an extended period of time and will not have access to electric wires, they must use a transportable and inexhaustible source of energy, and solar panels are one of the best options for floating buoys. Temperature fluctuations affect the performance of photovoltaic cells, and because we have the phenomenon of surface evaporation on the surface of the oceans and lakes, this phenomenon affects the modules and frames of the solar cell and reduces its temperature. As a result, the panel's performance and efficiency suffer. As a result, modeling and simulation of cells prior to embedding them on floating buoys is critical. Using diode equivalent circuits is one of the most prevalent modeling methods, and as described in the article, we were able to achieve very precise and positive results by using the single diode model and the ACO algorithm, so that the RMSE was reduced. In 2.46 seconds per iteration, a value of 5.2217×10^{-5} was achieved after 30 runs. This modeling and its outcomes are the most consistent with real-world cell behaviors and graphs. According to the research, the ant colony algorithm employed in this article is superior and more accurate than most algorithms, making it one of the most efficient algorithms in the modeling of solar panels used in buoys.

REFERENCES

[1]   S. Guo, Y. Zheng, and L. Gan, "The design and application of intelligent buoys in polar water," in *Proceedings of the 2018 7th International Conference on Energy, Environment and Sustainable Development (ICEESD 2018)*, 2018, pp. 1419–1424, doi: 10.2991/iceesd-18.2018.258.

[2]   S. Falleni *et al.*, "Design, development, and testing of a smart buoy for underwater testbeds in shallow waters," in *Global Oceans 2020: Singapore – U.S. Gulf Coast*, Oct. 2020, pp. 1–7, doi: 10.1109/IEEECONF38699.2020.9389065.

[3]   R. H. Rozali *et al.*, "Floating buoy technology for research purposes," *International Journal of Innovative Technology and Exploring Engineering*, vol. 8, no. 12, pp. 5514–5520, Oct. 2019, doi: 10.35940/ijitee.L3967.1081219.

[4]   T. J. Smyth, J. R. Fishwick, C. P. Gallienne, J. A. Stephens, and A. J. Bale, "Technology, design, and operation of an autonomous

buoy system in the western English channel," *Journal of Atmospheric and Oceanic Technology*, vol. 27, no. 12, pp. 2056–2064, Dec. 2010, doi: 10.1175/2010JTECHO734.1.

[5] N. Kannan and D. Vakeesan, "Solar energy for future world: A review," *Renewable and Sustainable Energy Reviews*, vol. 62, pp. 1092–1105, Sep. 2016, doi: 10.1016/j.rser.2016.05.022.

[6] J. Chen, Y. Li, X. Zhang, and Y. Ma, "Simulation and design of solar power system for ocean buoy," *Journal of Physics: Conference Series*, vol. 1061, Jul. 2018, doi: 10.1088/1742-6596/1061/1/012018.

[7] A. Bahrami, S. Mohammadnejad, and S. Soleimaninezhad, "Photovoltaic cells technology: Principles and recent developments," *Optical and Quantum Electronics*, vol. 45, no. 2, pp. 161–197, Feb. 2013, doi: 10.1007/s11082-012-9613-9.

[8] L. El Chaar, L. A. Lamont, and N. El Zein, "Review of photovoltaic technologies," *Renewable and Sustainable Energy Reviews*, vol. 15, no. 5, pp. 2165–2175, Jun. 2011, doi: 10.1016/j.rser.2011.01.004.

[9] P. K. Nayak, S. Mahesh, H. J. Snaith, and D. Cahen, "Photovoltaic solar cell technologies: analysing the state of the art," *Nature Reviews Materials*, vol. 4, no. 4, pp. 269–285, Mar. 2019, doi: 10.1038/s41578-019-0097-0.

[10] T. Dittrich, *Materials concepts for solar cells*. World Scientific (Europe), 2018, doi: 10.1142/q0131.

[11] M. F. AlHajri, K. M. El-Naggar, M. R. AlRashidi, and A. K. Al-Othman, "Optimal extraction of solar cell parameters using pattern search," *Renewable Energy*, vol. 44, pp. 238–245, Aug. 2012, doi: 10.1016/j.renene.2012.01.082.

[12] X. Chen, B. Xu, C. Mei, Y. Ding, and K. Li, "Teaching–learning–based artificial bee colony for solar photovoltaic parameter estimation," *Applied Energy*, vol. 212, pp. 1578–1588, Feb. 2018, doi: 10.1016/j.apenergy.2017.12.115.

[13] A. A. Z. Diab, H. M. Sultan, T. D. Do, O. M. Kamel, and M. A. Mossa, "Coyote optimization algorithm for parameters estimation of various models of solar cells and PV modules," *IEEE Access*, vol. 8, pp. 111102–111140, 2020, doi: 10.1109/ACCESS.2020.3000770.

[14] A. R. Jordehi, "Parameter estimation of solar photovoltaic (PV) cells: A review," *Renewable and Sustainable Energy Reviews*, vol. 61, pp. 354–371, Aug. 2016, doi: 10.1016/j.rser.2016.03.049.

[15] M.-N. Khursheed, M. F. Nadeem Khan, G. Ali, and A. K. Khan, "A review of estimating solar photovoltaic cell parameters," in *2019 2nd International Conference on Computing, Mathematics and Engineering Technologies (iCoMET)*, Jan. 2019, pp. 1–6, doi: 10.1109/ICOMET.2019.8673500.

[16] X. Lin and Y. Wu, "Parameters identification of photovoltaic models using niche-based particle swarm optimization in parallel computing architecture," *Energy*, vol. 196, Apr. 2020, doi: 10.1016/j.energy.2020.117054.

[17] C. Blum, "Ant colony optimization: Introduction and recent trends," *Physics of Life Reviews*, vol. 2, no. 4, pp. 353–373, Dec. 2005, doi: 10.1016/j.plrev.2005.10.001.

[18] M. Dorigo, M. Birattari, and T. Stutzle, "Ant colony optimization," *IEEE Computational Intelligence Magazine*, vol. 1, no. 4, pp. 28–39, Nov. 2006, doi: 10.1109/MCI.2006.329691.

[19] M. Dorigo and C. Blum, "Ant colony optimization theory: A survey," *Theoretical Computer Science*, vol. 344, no. 2–3, pp. 243–278, Nov. 2005, doi: 10.1016/j.tcs.2005.05.020.

[20] M. Dorigo and T. Stützle, *Ant colony optimization*. The MIT Press, 2004, doi: 10.7551/mitpress/1290.001.0001.

[21] D. Wilson, "The chesapeake bay interpretive buoy system: Recent expansion and advances," in *OCEANS 2009*, Oct. 2009, pp. 1–5, doi: 10.23919/OCEANS.2009.5422353.

[22] L. Li, G. Xiong, X. Yuan, J. Zhang, and J. Chen, "Parameter extraction of photovoltaic models using a dynamic self-adaptive and mutual- comparison teaching-learning-based optimization," *IEEE Access*, vol. 9, pp. 52425–52441, 2021, doi: 10.1109/ACCESS.2021.3069748.

[23] B. Lekouaghet, A. Boukabou, and C. Boubakir, "Estimation of the photovoltaic cells/modules parameters using an improved rao-based chaotic optimization technique," *Energy Conversion and Management*, vol. 229, Feb. 2021, doi: 10.1016/j.enconman.2020.113722.

[24] J. Ma, K. L. Man, T. O. Ting, N. Zhang, S.-U. Guan, and P. W. H. Wong, "Approximate single-diode photovoltaic model for efficient I-V characteristics estimation," *The Scientific World Journal*, vol. 2013, pp. 1–7, 2013, doi: 10.1155/2013/230471.

[25] V. J. Chin, Z. Salam, and K. Ishaque, "Cell modelling and model parameters estimation techniques for photovoltaic simulator application: A review," *Applied Energy*, vol. 154, pp. 500–519, Sep. 2015, doi: 10.1016/j.apenergy.2015.05.035.

[26] M. Abd Elaziz and D. Oliva, "Parameter estimation of solar cells diode models by an improved opposition-based whale optimization algorithm," *Energy Conversion and Management*, vol. 171, pp. 1843–1859, Sep. 2018, doi: 10.1016/j.enconman.2018.05.062.

[27] A. A. Z. Diab, H. M. Sultan, R. Aljendy, A. S. Al-Sumaiti, M. Shoyama, and Z. M. Ali, "Tree growth based optimization algorithm for parameter extraction of different models of photovoltaic cells and modules," *IEEE Access*, vol. 8, pp. 119668–119687, 2020, doi: 10.1109/ACCESS.2020.3005236.

[28] N. F. Abdul Hamid, N. A. Rahim, and J. Selvaraj, "Solar cell parameters extraction using particle swarm optimization algorithm," in *2013 IEEE Conference on Clean Energy and Technology (CEAT)*, Nov. 2013, pp. 461–465, doi: 10.1109/CEAT.2013.6775676.

[29] D. Yousri, S. B. Thanikanti, D. Allam, V. K. Ramachandaramurthy, and M. B. Eteiba, "Fractional chaotic ensemble particle swarm optimizer for identifying the single, double, and three diode photovoltaic models' parameters," *Energy*, vol. 195, Mar. 2020, doi: 10.1016/j.energy.2020.116979.

[30] J. Bai, S. Liu, Y. Hao, Z. Zhang, M. Jiang, and Y. Zhang, "Development of a new compound method to extract the five parameters of PV modules," *Energy Conversion and Management*, vol. 79, pp. 294–303, Mar. 2014, doi: 10.1016/j.enconman.2013.12.041.

[31] M. A. Mughal, Q. Ma, and C. Xiao, "Photovoltaic cell parameter estimation using hybrid particle swarm optimization and simulated annealing," *Energies*, vol. 10, no. 8, Aug. 2017, doi: 10.3390/en10081213.

[32] V. Nazerian and S. Babaei, "Optimization of exponential double-diode model for photovoltaic solar cells using GA-PSO algorithm," *Lecture Notes in Electrical Engineering*, vol. 480, pp. 697–703, 2019, doi: 10.1007/978-981-10-8672-4_52.

[33] M. Dorigo, E. Bonabeau, and G. Theraulaz, "Ant algorithms and stigmergy," *Future Generation Computer Systems*, vol. 16, no. 8, pp. 851–871, Jun. 2000, doi: 10.1016/S0167-739X(00)00042-X.

[34] M. Dorigo and G. Di Caro, "Ant colony optimization: a new meta-heuristic," in *Proceedings of the 1999 Congress on Evolutionary Computation-CEC99 (Cat. No. 99TH8406)*, 1999, pp. 1470–1477, doi: 10.1109/CEC.1999.782657.

[35] S. Mirjalili, *Evolutionary algorithms and neural networks - theory and applications (studies in computational intelligence)*, vol. 780. Cham: Springer; 1st ed., 2019.

[36] M. Dorigo and T. Stützle, "The ant colony optimization metaheuristic: Algorithms, applications, and advances," in *Handbook of Metaheuristics*, 2003, pp. 250–285, doi: 10.1007/0-306-48056-5_9.

[37] V. Maniezzo and A. Carbonaro, *Ant colony optimization: An overview*. Boston, MA: Springer US, 2002.

[38] A. Romeo and E. Artegiani, "CdTe-based thin film solar cells: Past, present and future," *Energies*, vol. 14, no. 6, Mar. 2021, doi: 10.3390/en14061684.

[39] K. Yu, B. Qu, C. Yue, S. Ge, X. Chen, and J. Liang, "A performance-guided JAYA algorithm for parameters identification of photovoltaic cell and module," *Applied Energy*, vol. 237, pp. 241–257, Mar. 2019, doi: 10.1016/j.apenergy.2019.01.008.

[40] D. Oliva, E. Cuevas, and G. Pajares, "Parameter identification of solar cells using artificial bee colony optimization," *Energy*, vol. 72, pp. 93–102, Aug. 2014, doi: 10.1016/j.energy.2014.05.011.

[41] D. Oliva, M. Abd El Aziz, and A. Ella Hassanien, "Parameter estimation of photovoltaic cells using an improved chaotic whale optimization algorithm," *Applied Energy*, vol. 200, pp. 141–154, Aug. 2017, doi: 10.1016/j.apenergy.2017.05.029.

[42] S. Xu and Y. Wang, "Parameter estimation of photovoltaic modules using a hybrid flower pollination algorithm," *Energy Conversion and Management*, vol. 144, pp. 53–68, Jul. 2017, doi: 10.1016/j.enconman.2017.04.042.

[43] K. Yu, X. Chen, X. Wang, and Z. Wang, "Parameters identification of photovoltaic models using self-adaptive teaching-learning-based optimization," *Energy Conversion and Management*, vol. 145, pp. 233–246, 2017, doi: 10.1016/j.enconman.2017.04.054.

[44] A. R. Jordehi, "Enhanced leader particle swarm optimisation (ELPSO): An efficient algorithm for parameter estimation of photovoltaic (PV) cells and modules," *Solar Energy*, vol. 159, pp. 78–87, Jan. 2018, doi: 10.1016/j.solener.2017.10.063.

[45] A. M. Beigi and A. Maroosi, "Parameter identification for solar cells and module using a hybrid firefly and pattern search algorithms," *Solar Energy*, vol. 171, pp. 435–446, Sep. 2018, doi: 10.1016/j.solener.2018.06.092.

[46] K. Yu, J. J. Liang, B. Y. Qu, Z. Cheng, and H. Wang, "Multiple learning backtracking search algorithm for estimating parameters of photovoltaic models," *Applied Energy*, vol. 226, pp. 408–422, Sep. 2018, doi: 10.1016/j.apenergy.2018.06.010.

[47] A. Askarzadeh and A. Rezazadeh, "Artificial bee swarm optimization algorithm for parameters identification of solar cell models," *Applied Energy*, vol. 102, pp. 943–949, Feb. 2013, doi: 10.1016/j.apenergy.2012.09.052.

[48] A. R. Jordehi, "Time varying acceleration coefficients particle swarm optimisation (TVACPSO): A new optimisation algorithm for estimating parameters of PV cells and modules," *Energy Conversion and Management*, vol. 129, pp. 262–274, Dec. 2016, doi: 10.1016/j.enconman.2016.09.085.

[49] W. Long, S. Cai, J. Jiao, M. Xu, and T. Wu, "A new hybrid algorithm based on grey wolf optimizer and cuckoo search for parameter extraction of solar photovoltaic models," *Energy Conversion and Management*, vol. 203, Jan. 2020, doi: 10.1016/j.enconman.2019.112243.

[50] S. Jiao *et al.*, "Orthogonally adapted Harris hawks optimization for parameter estimation of photovoltaic models," *Energy*, vol. 203, Jul. 2020, doi: 10.1016/j.energy.2020.117804.

[51] L. M. P. Deotti, J. L. R. Pereira, and I. C. da Silva Júnior, "Parameter extraction of photovoltaic models using an enhanced Lévy flight bat algorithm," *Energy Conversion and Management*, vol. 221, Oct. 2020, doi: 10.1016/j.enconman.2020.113114.

BIOGRAPHIES OF AUTHORS

Vahdat Nazerian received his B.Sc. degree from Iran University of Science and Technology, Tehran, Iran in 2003, M.Sc. and Ph.D. degrees from Khaje Nasir Toosi University of Technology, Tehran, Iran in 2005 and 2011, respectively, all in Electronics. He joined the Electrical Engineering Department of the University of Mazandaran in 2014 as an assistant professor. His research and teaching concern semiconductor devices, analysis and fabrication. His research presently focuses on soft-computing, intelligent network, nanotechnology and application, renewable energy, and optimization algorithms. He can be contacted at email: v.nazerian@umz.ac.ir.

Hossein Asadollahi received his B.Sc. degree in Electrical and Electronics Engineering at the University of Mazandaran in January 2022. He has been pursuing the M.Sc. degree in Telecommunications Systems Engineering at Tarbiat Modares University since September 2022. His research interests include renewable energies, as well as wireless communications, mobile network location, and optimization algorithms. He has conducted extensive research in the field of renewable energies and is committed to exploring new ways of harnessing sustainable energy sources. He can be contacted at email: h.asadollahi43@umail.umz.ac.ir.

Tole Sutikno is a lecturer, and serves as the head of the Electrical Engineering Department, as well as the head of the Master Program of Electrical Engineering within the Faculty of Industrial Technology at Universitas Ahmad Dahlan (UAD) in Yogyakarta, Indonesia. In 1999, 2004, and 2016, he graduated with a Bachelor of Engineering from Universitas Diponegoro, a Master of Engineering from Universitas Gadjah Mada, and a Doctor of Philosophy in Electrical Engineering from Universiti Teknologi Malaysia. All three degrees are in the field of electrical engineering. Since the year 2008, he has held the position of Associate Professor at the Universitas Ahmad Dahlan in Yogyakarta, Indonesia. He is among the top 2% of researchers named by Stanford University and Elsevier BV as the most influential scientists in the world for 2021–present. His research interests include the areas of digital design, industrial applications, industrial electronics, industrial informatics, power electronics, motor drives, renewable energy, FPGA applications, embedded systems, artificial intelligence, intelligent control, digital libraries, and information technology. He can be contacted at email: tole@te.uad.ac.id.